Unraveling the Broadband Emission in Mixed Tin-Lead Layered Perovskites

ADVANCED OPTICAL MATERIALS
www.advopticalmat.de

Unraveling the Broadband Emission in Mixed Tin-Lead Layered Perovskites

Hong-Hua Fang, Eelco K. Tekelenburg, Haibo Xue, Simon Kahmann, Lijun Chen, Sampson Adjokatse, Geert Brocks, Shuxia Tao, and Maria Antonietta Loi**

Low-dimensional halide perovskites with broad emission are a hot topic for their promising application as white light sources. However, the physical origin of this broadband emission in the sub-bandgap region is still controversial. This work investigates the broad Stokes-shifted emission bands in mixed lead-tin 2D perovskite films prepared by mixing precursor solutions of phenethylammonium lead iodide (PEA_2PbI_4, PEA = phenethylammonium) and phenethylammonium tin iodide (PEA_2SnI_4). The bandgap can be tuned by the lead-tin ratio, whereas the photoluminescence is broad and significantly Stokes-shifted and appears to be fairly insensitive to the relative amount of Pb and Sn. It is experimentally observed that these low-dimensional systems show substantially less bandgap bowing than their 3D counterpart. Theoretically, this can be attributed to the smaller spin–orbit coupling effect on the 2D perovskites compared to that of 3D ones. The time-resolved photoluminescence shows an ultrafast decay in the high-energy range of the spectra that coincides with the emission range of PEA_2SnI_4, while the broadband emission decay is slower, up to the microsecond range. Sub-gap photoexcitation experiments exclude exciton self-trapping as the origin of the broadband emission, pointing to defects as the origin of the broadband emission in 2D Sn/Pb perovskite alloys.

1. Introduction

Two-dimensional metal-halide Ruddlesden–Popper perovskites (RPP) have become increasingly prevalent in the past few years due to their great potential in optoelectronic applications, such as solar cells,[1–3] light-emitting diodes,[4] lasers,[5] and X-ray detectors.[6] Compared to their 3D counterparts, the dielectric and quantum confinement effect in 2D perovskites play an essential role in their optical and electrical properties, leading to strong excitonic effects and rich exciton physics (including biexcitons and trions).[7–13] Thus, the luminescence of these layered compounds is typically dominated by a narrow-band free exciton emission. Interestingly, instead of narrow-band photoluminescence, an increasing number of systems, such as (*N*-MEDA)$PbBr_4$ (*N*-MEDA = N^1-methylethane-1,2-diammonium) and (EDBE)PbX_4 (EDBE = 2,2′-(ethylenedioxy)-bis-(ethylammonium)), show broadband emission with a large Stokes shift.[14–19] Some of them emit photons across the entire visible spectrum, affording broadband white light emission. In some compounds, the broad emission exhibits high photoluminescence (PL) quantum yield (>45%),[20] offering the possibility of solid lighting applications.

Accompanying the research progress on these broadband emitters, significant theoretical work has been addressing its origin. Self-trapped excitons (STEs) are generally considered

H.-H. Fang, M. A. Loi
State Key Laboratory of Precision Measurement Technology and Instruments
Department of Precision Instrument
Tsinghua University
Beijing 100084, China
E-mail: hfang@mail.tsinghua.edu.cn; m.a.loi@rug.nl

H.-H. Fang, E. K. Tekelenburg, S. Kahmann, L. Chen, S. Adjokatse
Photophysics & OptoElectronics
Zernike Institute for Advanced Materials
University of Groningen
Nijenborgh 4, Groningen 9747 AG, The Netherlands

H. Xue, G. Brocks, S. Tao
Materials Simulation and Modelling
Department of Applied Physics
Eindhoven University of Technology
Eindhoven 5600 MB, The Netherlands

H. Xue, G. Brocks, S. Tao
Center for Computational Energy Research
Department of Applied Physics
Eindhoven University of Technology
Eindhoven 5600 MB, The Netherlands

S. Kahmann
Cavendish Laboratory
University of Cambridge
JJ Thomson Avenue, Cambridge CB30HE, UK

G. Brocks
Computational Materials Science, Faculty of Science and Technology and MESA+ Institute for Nanotechnology
University of Twente
Enschede 7500AE, The Netherlands

The ORCID identification number(s) for the author(s) of this article can be found under https://doi.org/10.1002/adom.202202038.

DOI: 10.1002/adom.202202038

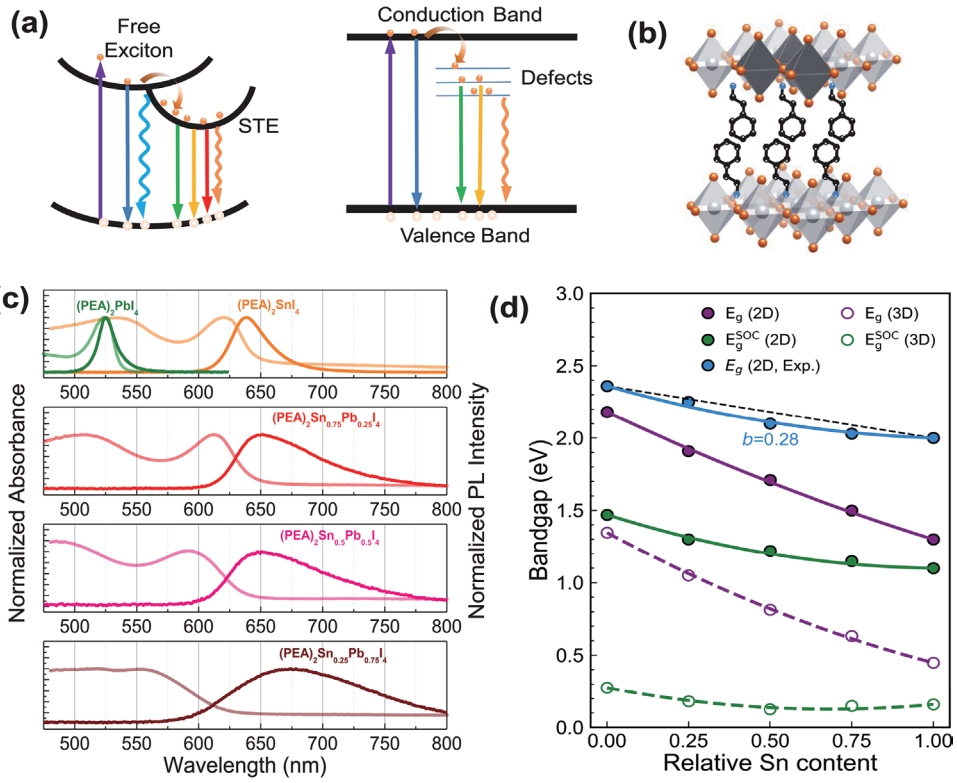

Figure 1. a) Mechanism for subgap broad emission in perovskite. b) Illustration of the crystal structure of mixed $PEA_2Sn_xPb_{1-x}I_4$. c) UV–vis absorption and photoluminescence spectra of neat PEA_2SnI_4, PEA_2PbI_4, and mixed $PEA_2Sn_xPb_{1-x}I_4$. d) Experimental and calculated bandgaps, without and with SOC, as a function of Sn content x in $PEA_2Sn_xPb_{1-x}I_4$. The circles are calculated bandgap energies; the dashed black line is a linear line connecting two ends; colored lines are fitted quadratic curves, with bowing parameters, b. The bandgap values of the 3D perovskite $FASn_xPb_{1-x}I_3$ are reproduced from ref. [43].

the leading cause determining the experimental feature.[21–26] In this scenario, charge carriers couple to the soft lattice, inducing elastic structural distortions that lower the system's energy, as shown in **Figure 1**a.[27] Because of their transient quasiparticle nature, an STE cannot be directly excited from the ground state by the below-gap light.[25,28] This process can be intrinsic (self-tapped states can be regarded as excited states that occur due to transient elastic lattice deformation upon illumination) or extrinsic (initial local potential wells in a host material serve as a nucleating site for subsequent self-trapping events). However, self-trapping is not the only mechanism for inducing broad photoluminescence; permanent structural defects and dopants can induce in-gap states and broaden the emission (Figure 1a).[28–30] In these cases, excitons are assumed to be trapped in an in-gap state, resulting in a Stokes shifted emission. Since the in-gap state and STEs share very similar features in luminescence characteristics, they have rarely been disentangled.

Thus far, most reported 2D perovskites with broadband emissions are lead-based with a special selection of amine spacer.[14,15,31] Recently, broadband emissions from mixed divalent metal 2D perovskites have been reported.[25,29,32,33] Tin (II) has been considered the most suitable candidate for Pb^{2+} replacement because of their similar electronic states with lone-pair orbitals.[34–39] Therefore, the substitution of Pb^{2+} by Sn^{2+} is expected to give rise to a minimal perturbation in the lattice structure. This is promising for lead-free devices.[38,40,41] Interestingly, mixed tin-lead 2D perovskites show distinctive properties from their 3D counterpart, where band-edge emission always dominates the spectra. For instance, Yu et al. observed a pronounced broadband luminescence ranging from the red to NIR region in Sn-doped PEA_2PbI_4 (PEA = phenethylammonium).[29] The authors ascribed the radiative decay to tin-triggered extrinsic STEs. In contrast, Hu et al. reported that the red-shifted broad emission could be due to PEA_2PbI_4:PEA_2SnI_4 interfaces in thin films, as demonstrated in mechanically fabricated double-layered PEA_2PbI_4/PEA_2SnI_4 heterostructures.[32] Kuang et al. recently pointed that there are two independent STEs emitters in Pb–Sn alloyed single crystals, $(C_{10}NH_{22})_2Pb_{1-x}Sn_xBr_4$.[33] In this regard, the photogenerated species in the mixed Pb–Sn perovskite and the formation process of broad emission bands remain controversial. Therefore, more in-depth investigations are required to understand the true origin of the broad light emission in these materials.

In this paper, we prepared perovskite thin films by mixing precursor solutions of PEA_2PbI_4 and PEA_2SnI_4 and closely examined their optical properties at varying temperatures. We show the presence of a broad and strongly Stokes-shifted emission band in all mixtures. Through a combination of temperature-dependent steady-state and time-resolved photoluminescence investigations, we provide insight into the origin of the broadband emission in these materials. Our experimental results point to the fact that intrinsic self-trapping is

not responsible for the broad emission in these mixtures, but the broad emission is to be attributed to defect-induced luminescence.

2. Results and Discussion

The absorption and photoluminescence spectra of the polycrystalline thin films are presented in Figure 1c. For simplicity, the mixed Sn–Pb perovskites are named by the precursor Sn:Pb ratio. The absorption onset of the mixed $PEA_2Sn_xPb_{1-x}I_4$ perovskites can be tuned by the precursor Sn:Pb ratio. PEA_2PbI_4 and PEA_2SnI_4 exhibit large exciton binding energy (≈100 s meV), giving rise to their strong excitonic absorption peak at 524 and 621 nm, respectively.[12] We note that the mixed perovskite thin-film shows absorption peaks, which vary from 613 to 560 nm when the lead content increases from 0.25 to 0.75, as shown in Figure 1c. This behavior implies that the material's bandgap can be tuned by the mixture ratio.

Interestingly, instead of the well-known unusual bandgap changes in 3D mixed Pb–Sn perovskites, in which the mixed compositions display smaller bandgaps than that of the smallest of the two parent systems,[34] we observe only a mild tunability in the 2D systems (Figure 1d). This can be reflected by the much smaller bowing parameter for 2D perovskite (0.28) compared to that of 3D counterparts (0.89).[42] To understand this difference, we calculate the evolution of bandgaps of the mixed perovskites with and without spin–orbit coupling (SOC), using density functional theory (DFT) calculations. In Figure 1d, without SOC, bandgaps of 2D systems are consistently larger than 3D counterparts by about 0.86 eV regardless of the compositions. With SOC, bandgaps of all perovskites decrease, but the effect on 2D compounds is smaller than that on 3D counterparts and is more pronounced for Pb-based perovskites (0.71 eV for 2D vs 1.07 for 3D) than Sn-based ones (0.20 eV for 2D vs 0.29 eV for 3D). These factors together lead to a situation where the bandgap difference between Pb- and Sn-based 2D perovskites is relatively large so that only mild changes/bowing in bandgaps can occur in the mixed compounds.

We next investigate the photoluminescence behavior of the mixtures. The PL peak position is red-shifted when compared to the lead or tin-based systems (PEA_2PbI_4, 525 nm; and PEA_2SnI_4 637 nm), resulting in a Stokes shift of 100 nm for $PEA_2Pb_{0.75}Sn_{0.25}I_4$, while it is only 15 nm for pure PEA_2SnI_4 and negligible for PEA_2PbI_4. Moreover, the mixed perovskite exhibits broadband emission with a full width at half maximum (FWHM) of ≈100 nm, in contrast to the narrow emission from pure thin films. Contrary to the absorption, the photoluminescence peak slightly shifts from 650 to 675 nm as the lead content increases from 0.25 to 0.75. Interestingly, we observed an increased Stokes shift with a high-lead content.

A very long photoluminescence lifetime is measured in the mixtures, with the emission measured at the PL peak extending over hundreds of nanoseconds. In contrast, the pure parent samples possess a relatively short average photoluminescence lifetime (0.48 ns for the Sn system and 0.5 ns for Pb one, see Figure S1, Supporting Information). We postulate that the longer photoluminescence lifetime originates from the reversible processes of multiple trapping and detrapping of carriers at the sub-bandgap in the mixture.[43] The process of electron thermal detrapping back to the emissive state detrapped contributes to the delayed emission of photons up to several hundred nanoseconds after photoexcitation.

To probe the origin of the broad emission, we conducted temperature-dependent PL measurements of all samples in the range from 5.6 to 295 K. **Figure 2** shows the temperature-dependent PL spectra of $PEA_2Sn_xPb_{1-x}I_4$ and PEA_2SnI_4. With the decrease in temperature, PL linewidth narrowing and enhancement of the emission intensity are observed for all samples. Moreover, the most prominent PL peak red shifts continuously up to 675 nm for PEA_2SnI_4, 700 nm for $PEA_2Sn_{0.25}Pb_{0.75}I_4$, 706 nm for $PEA_2Sn_{0.5}Pb_{0.5}I_4$, and 710 nm for $PEA_2Sn_{0.75}Pb_{0.25}I_4$ at 5.6 K. Furthermore, also as noticed for room temperature, the broad emission band for the mixed samples is located at a similar position in wavelength. This implies that they share an identical mechanism, as discussed below.

We proceed to compare the low-temperature absorption and photoluminescence spectra of our samples. As illustrated in **Figure 3** and Figure S2 (Supporting Information), all samples' optical absorption spectra have distinct excitonic features typical of RPP samples, with increased exciton absorption energy when the lead content increases. As mentioned earlier, the emission peaks at 5.6 K for the mixed $PEA_2Sn_xPb_{1-x}I_4$ perovskites are pinned around 700 nm showing only a slight variation with lead content). Interestingly, in the PL spectra of $PEA_2Pb_{0.5}Sn_{0.5}I_4$ and $PEA_2Pb_{0.25}Sn_{0.75}I_4$, a small shoulder structure can be observed at the higher energy side of the emission peak in addition to the broadband emission. This fine substructure could be linked to the emission from neat PEA_2SnI_4, given the spectral range of 650–680 nm, as indicated in Figure S3 (Supporting Information). We named this part component A, and the broad, strong emission component B.

It is worth highlighting that the room temperature PL spectra can be fitted by two main components similar to the spectra at 5.6 K: one stems from the emission of PEA_2SnI_4, the other with broad width is centered at around 675 nm. The ratio between these two components is associated with the lead content. As the lead content increases, the component B becomes more dominant, as seen for $PEA_2Pb_{0.25}Sn_{0.75}I_4$.

Notably, our component B exhibits a broad emission feature similar to the previously reported STEs in PEA_2PbI_4, where a trace amount of Sn (0.00005%) dopant was said to trigger the occurrence of exciton self-trapping.[29] In this mechanism, once electrons and holes are photogenerated, they will quickly self-trap from a free exciton (FE) to a self-trapped state (STE).[25] To further elucidate if this is the underlying mechanism at the origin of component B, we used photons of below-bandgap energy to probe its nature, which is recently reported to distinguish defect luminescence and defect-assisted STE luminescence.[28,30,44] Herein, we used excitation wavelengths of 500 and 660 nm to compare the above and below-bandgap excitation.

Interestingly, we observed identical luminescence spectra from the low-energy broad emission in $PEA_{25}Sn_{0.25}Pb_{0.7}I_4$, $PEA_2Sn_{0.5}Pb_{0.5}I_4$, and $PEA_2Pb_{0.25}Sn_{0.75}I_4$ (Figures S4–S6, Supporting Information) independent of above or below-gap excitation. This key observation questions the importance of STEs in our mixed compounds. Furthermore, we measured

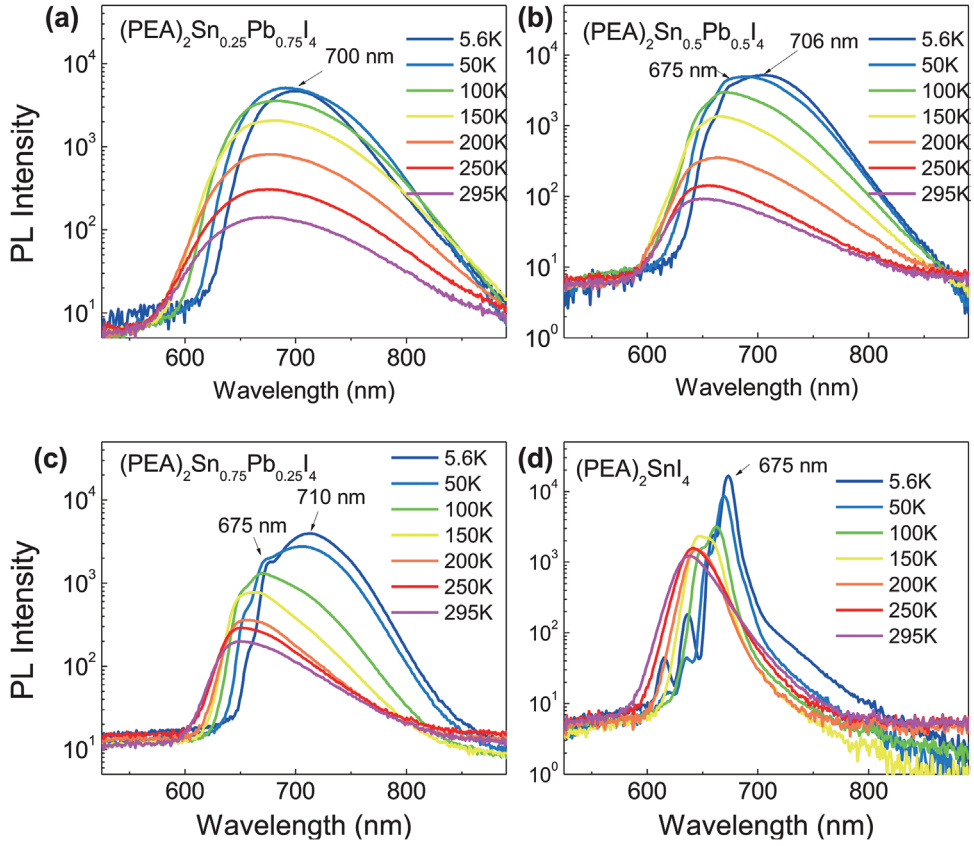

Figure 2. Temperature-dependent photoluminescence spectra of mixed $PEA_2Sn_xPb_{1-x}I_4$. a) $PEA_2Sn_{0.25}Pb_{0.75}I_4$, b) $PEA_2Sn_{0.5}Pb_{0.5}I_4$, c) $PEA_2Sn_{0.75}Pb_{0.25}I_4$, and d) neat PEA_2SnI_4.

the power-dependent PL with an excitation of 660 nm. From these measurements, an intensity-dependence slope of 0.97 for $PEA_2Pb_{0.25}Sn_{0.75}I_4$ and 1.15 for $PEA_2Pb_{0.75}Sn_{0.25}I_4$ (see Figures S4–S6, Supporting Information) is resulting. This important control experiment verifies the absence of two-photon processes and highlights that there are optically accessible states sub-bandgap in the mixed systems. As STE cannot be excited through below-bandgap photon energies, we exclude intrinsic STE as the origin of observed broadband emission.

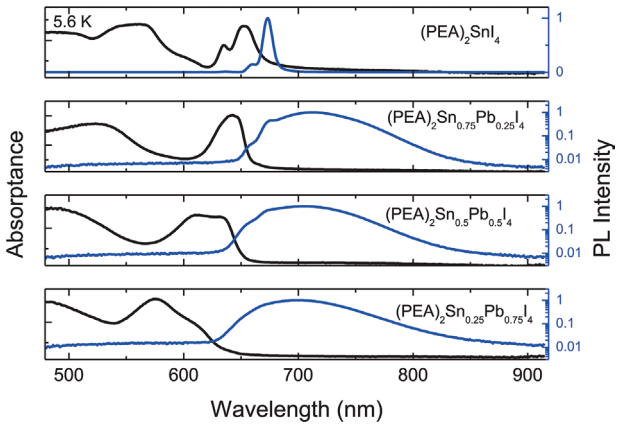

Figure 3. UV–vis absorption and photoluminescence spectra of neat PEA_2SnI_4 and mixed $PEA_2Sn_xPb_{1-x}I_4$ at 5.6 K.

A very plausible scenario for this broadband emission is defect-mediated low-energy emission. Several early studies show that the formation energy of tin-related defects is low in tin-based or mixed lead-tin perovskite.[45–47] Furthermore, the low-temperature solution process could introduce structural disorder. Thus, the concentration of defects can be very high. That is a possible reason we did not observe a saturation signature in power-dependent PL measurement with a carrier density approaching 10^{19} cm^{-3} (see Figures S4, S6, and S7, Supporting Information). However, the defects in the mixture may deteriorate photoluminescence efficiency by introducing non-radiative recombination, which is proved by lower relative PL intensity in the mixed perovskites (see Figure S8, Supporting Information).

Recently, Zhang and co-workers reported that charge transfer states could be effectively formed in heterostructures of RPP prepared by mixing PEA_2PbI_4:PEA_2SnI_4 crystal.[32] It is envisaged that the domains of PEA_2SnI_4 and PEA_2PbI_4 may occur because the tin and lead compounds have different Gibbs free energies of formation leading to the heterostructures.[48–50] In this picture, low-energy luminescence would stem from a charge-transfer state formed by electron–hole coupling between two chemically different domains.

To clear this doubt, we performed XRD measurements on our thin films. As indicated in Figure S9 (Supporting Information), increasing Sn content shifts the peak to larger two-theta, as expected from the smaller size of Sn compared to Pb. In

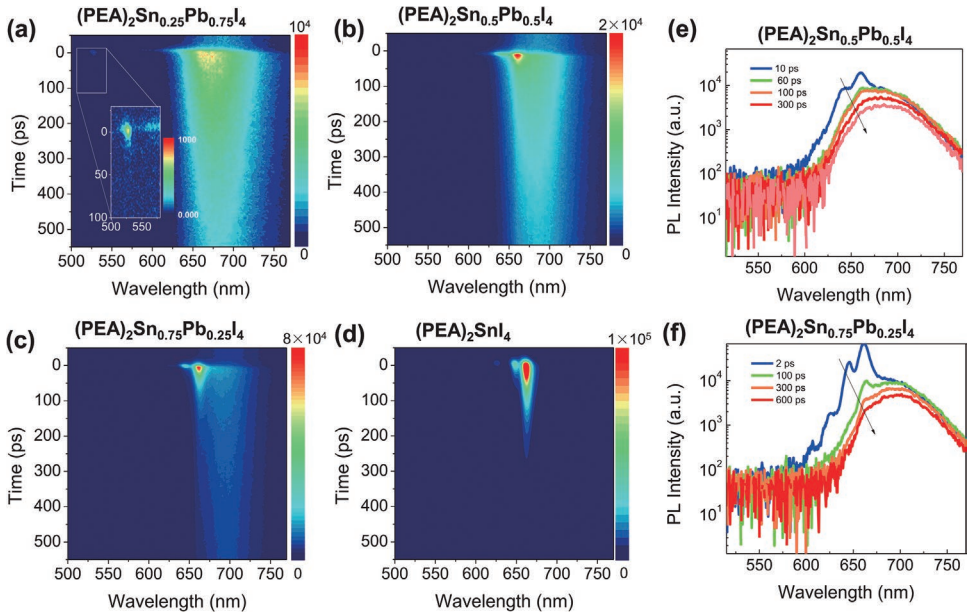

Figure 4. 2D pseudo-color plot of time-resolved photoluminescence spectra of mixed $PEA_2Sn_xPb_{1-x}I_4$ perovskite: a) $PEA_2Sn_{0.25}Pb_{0.75}I_4$, b) $PEA_2Sn_{0.5}Pb_{0.5}I_4$, c) $PEA_2Sn_{0.75}Pb_{0.25}I_4$, and d) neat PEA_2SnI_4. e,f) Photoluminescence spectra of $PEA_2Sn_{0.5}Pb_{0.5}I_4$ and $PEA_2Sn_{0.75}Pb_{0.25}I_4$. after varying delayed time after photoexcitation.

the meantime, the peaks keep the same widths. This excludes that separate PEA_2PbI_4 and PEA_2SnI_4 domains are the dominant phases as it should increase the width of the peaks due to the convolution of the peaks corresponding to PEA_2PbI_4 and PEA_2SnI_4. Additionally, the luminescence of the thin film shows clear uniformity in optical properties. When checking the absorbance, the shift of the excitonic peak indicates that the majority of the material is a Pb:Sn alloyed phase. Thus, the broadband emission from charge-transfer states in our sample is less likely to occur. However, our alloys may contain small domains of PEA_2SnI_4. As observed in the low-temperature PL spectra of $PEA_2Sn_{0.75}Pb_{0.25}I_4$ and $PEA_2Sn_{0.25}Pb_{0.75}I_4$, the component A in PL spectra coincides with the optical transition from neat PEA_2SnI_4. This is possible because Sn-based perovskites usually undergo a rapid crystallization process,[40] this could lead to inclusion of PEA_2SnI_4 domains. We have to emphasize that inclusions of the neat compounds should be in the minority because component A in PL spectra is small in portion.

To further understand the recombination process, we examined the time-resolved photoluminescence of the thin films. **Figure 4** shows the 2D color plot of low-temperature time-resolved photoluminescence spectra in the mixed $PEA_2Sn_xPb_{1-x}I_4$ and the neat PEA_2SnI_4 film. As expected from the steady-state data, the photoluminescence of $PEA_2Sn_{0.75}Pb_{0.25}I_4$ and $PEA_2Sn_{0.5}Pb_{0.5}I_4$ is dominated by a broad signal with a fast component between 650 and 670 nm. Contrarily, the neat PEA_2SnI_4 film does not show any broad emission between 650 and 750 nm. The broad emission is consistent with the broad emission of component B in steady-state PL spectra. Component A decays quickly in time, while component B decays much slower. The lifetime of component B extends into the microsecond range (see Figure S10, Supporting Information). It is noteworthy that component A becomes more evident with increasing the Sn content in the early time window. This effect seems to be more pronounced at high excitation density (see Figure S7, Supporting Information). We also note that the high-energy emission increases in intensity upon continuous laser exposure (see Figures S12 and S13, Supporting Information). The appearance of the high energy peak seems origin from the photoinduced degradation effect. We observe that a luminescence peak at rang of 510–520 nm appears under high power continuous laser exposure, because the peak position is consistent with the emission peak of PEA_2PbI_4. Light-induced halide segregation has been widely reported in the mixed perovskite,[51] in our case, metal cation segregation is also possible explanation. Ultrafast photoluminescence dynamics show identical rise times for components A and B (Figure S11, Supporting Information). It is important to notice that we did not observe a strong correlation between components A and B, no time-dependent energy or charge transfer process is observed, suggesting that those are two independent states.

Overall, it should be no surprise that defects govern the photophysical characteristics of mixed lead-tin perovskite, especially considering that Sn(II) has the inherent propensity for oxidation.[36,39] This explains why samples are generally p-doped. On the other hand, it has been demonstrated from first-principles calculations that in hybrid 2D Sn/Pb perovskite alloys, the octahedral distortion caused by the organic spacer may further enhance the local structural relaxation effect.[52] In combination with defects, these factors play a role in carrier recombination and the resulting luminescence spectra.

3. Conclusion

In summary, we have investigated the photophysical properties of mixed lead-tin 2D perovskite thin films by combining transient

and steady-state photoluminescence spectroscopy. Mixing allows for tuning the bandgap energy although these low dimensional systems show substantially less bowing of the bandgap than the 3D counterpart. DFT calculations indicate that the milder bowing in 2D systems can be attributed to the smaller SOC effect on the 2D perovskites compared to that of 3D ones. We experimentally observed large Stokes-shifted broadband emissions in the mixed lead-tin systems. Time-resolved photoluminescence shows that this broadband emission has an extended decay up to the microsecond range. Below band-edge excitation excludes the formation of intrinsic self-trapped excitons as the origin of these broadband emissions. Defects in the mixture are the most plausibly responsible for the observed broadband emission.

4. Experimental Section

Materials: The perovskite films were prepared by spin coating from mixed two precursor solutions (PEA_2PbI_4 and PEA_2SnI_4). Thin films were cast on glass substrates, ultrasonically cleaned sequentially in detergent solution, deionized water, acetone, and isopropanol. After drying in an oven at 140 °C for at least 10 min, the substrates were treated with ultraviolet ozone for 20 min and immediately transferred into a nitrogen-filled glovebox for film deposition. The PEA_2PbI_4 perovskite precursor solution was prepared by dissolving PEAI (98.0% TCI) and PbI_2 (99.99% TCI) in a mixed solvent of anhydrous *N*, *N*-dimethylformamide (DMF), and anhydrous dimethylsulfoxide (DMSO) in a volume ratio of 4:1. The PEA_2SnI_4 precursor solutions were prepared by dissolving PEAI and tin (II) iodide (SnI2) precursors in a mixed solvent of DMF and DMSO (volume ratio 4:1). The solutions were stirred for at least 3 h at room temperature before deposition. The spin-coated films were fabricated using a two-step process with antisolvent treatment. The spin coating process uses 1000 rpm for 10 s followed by 4000 rpm for 30 s. 10 s prior to the end of the spin coating cycle, the antisolvent (chlorobenzene) was added to the film. In both cases, the films were immediately annealed at 100 °C.

Spectroscopic Measurements: The prepared thin films were mounted into a cryostat (Oxford Instruments Optistat CF) inside a nitrogen-filled glovebox without being exposed to air. The absorption measurements were carried out with a halogen lamp as a light source, and a Hamamatsu EM-CCD camera was used as the detector. PL spectra were measured by exciting the sample with 3.1 eV photons of the second harmonic of a mode-locked Ti: sapphire laser (Mira 900, Coherent). The laser power was adjusted using neutral density filters during the measurements. The excitation beam was spatially limited by an iris and focused with a 150 mm focal length lens. Steady-state spectra were collected using a Hamamatsu EM-CCD camera, and time-resolved traces were recorded using a Hamamatsu streak camera working in single sweep mode. Emitted photons were collected with a lens and directed to a spectrograph. A pulse picker was used to reduce the Ti:sapphire oscillator frequency (about 76 MHz) when needed for long-lived photoluminescence measurements.

Below-Bandgap Excitation: Excitation below the bandgap was performed using a supercontinuum laser (NKT Photonics SuperK Extreme, 76 MHz repetition rate, 1–2 ps pulse duration) as an excitation source. The photoluminescence was detected through a spectrograph (Shamrock SR303i, Andor) with 150 l mm^{-1} grating (800 nm blaze) equipped with a CCD camera (Luca R, Andor). Appropriate bandpass filters of 10 nm around the central wavelength of 500 nm for above gap excitation and 660 nm for below gap excitation were used in the excitation beam path to assure color purity. Two long-pass filters of with cutting wavelengths at 695 and 715 nm were used in the photoluminescence measurement to remove laser scattering and cut off the high-energy part of PL. Fluence-dependent measurements were carried out with a set of natural density filters.

Computational Methods: Density functional theory (DFT) calculations were performed with the Vienna Ab Initio simulation package (VASP),[53–55] employing the SCAN+rVV10 exchange-correlation functional[56] for electronic calculations and geometry optimization. The outermost s, p, and d (in the case of Pb and Sn) electrons were treated as valence electrons, whose interactions with the remaining ions were modeled by pseudopotentials generated within the projector-augmented wave (PAW) method.[57] The calculations used a plane wave kinetic energy cutoff of 450 eV, with a maximum cutoff energy of the plane-wave-basis set for all elements being 280 eV. The energy and force convergence criteria were set to 10^{-4} eV and 0.02 eV $Å^{-1}$, respectively. A $2 \times 2 \times 2$ supercell of PEA_2PbI_4[58] was used as the starting structure, based on which 1/4, 1/2, 3/4, and all of Pb atoms were replaced by Sn with a homogeneous distribution to simulate the mixed perovskite $PEA_2Sn_xPb_{1-x}I_4$. Lattice volume and ionic positions of all structures were fully relaxed, and the optimized structures are shown in Figure S14 (Supporting Information). Based on the optimized structures, electronic calculations were performed without and with spin–orbit coupling, respectively. The nonlinear bandgap (E_g) progression of the alloyed compound A_xB_{1-x} ($PEA_2Sn_xPb_{1-x}I_4$ in this case) follows the relation $E_g(PEA_2Sn_xPb_{1-x}I_4) = xE_g(PEA_2SnI_4) + (1-x)E_g(PEA_2PbI_4) - bx(1-x)$, with b being the so-called bowing parameter.[59–61]

Supporting Information

Supporting Information is available from the Wiley Online Library or from the author.

Acknowledgements

Arjen Kamp and Teodor Zaharia are thanked for their technical support. H.-H.F. acknowledges the financial support of the National Natural Science Foundation of China (Grant No: 62075115). S.K. is grateful for a research fellowship (Grant No: 408012143) awarded by the Deutsche Forschungsgemeinschaft (DFG). E.K.T. acknowledges the financial support of the Zernike Institute of Advanced Materials. This work was financed through the Materials for Sustainability (Mat4Sus) programme (739.017.005) of the Netherlands Organization for Scientific Research (NWO). This work is part of the research program of the Foundation for Fundamental Research on Matter (FOM), which is part of the Netherlands Organization for Scientific Research (NWO). This is a publication of the FOM focus Group "Next Generation Organic Photovoltaics" participating in the Dutch Institute for Fundamental Energy Research (DIFFER).

Conflict of Interest

The authors declare no conflict of interest.

Data Availability Statement

The data that support the findings of this study are available from the corresponding author upon reasonable request.

Keywords

bandgap bowing, defects, mixed lead-tin perovskite, Ruddlesden–Popper perovskites

Received: August 31, 2022
Revised: November 5, 2022
Published online: December 8, 2022

[1] S. Shao, J. Liu, G. Portale, H.-H. Fang, G. R. Blake, G. H. ten Brink, L. J. A. Koster, M. A. Loi, *Adv. Energy Mater.* **2018**, *8*, 1702019.
[2] D. Li, Y. Li, Z. Liu, D. Wang, S. F. Liu, *Sci. China: Technol. Sci.* **2021**, *64*, 1995.
[3] C. Liang, H. Gu, Y. Xia, Z. Wang, X. Liu, J. Xia, S. Zuo, Y. Hu, X. Gao, W. Hui, L. Chao, T. Niu, M. Fang, H. Lu, H. Dong, H. Yu, S. Chen, X. Ran, L. Song, B. Li, J. Zhang, Y. Peng, G. Shao, J. Wang, Y. Chen, G. Xing, W. Huang, *Nat. Energy* **2021**, *6*, 38.
[4] H. Tsai, W. Nie, J.-C. Blancon, C. C. Stoumpos, C. M. M. Soe, J. Yoo, J. Crochet, S. Tretiak, J. Even, A. Sadhanala, G. Azzellino, R. Brenes, P. M. Ajayan, V. Bulović, S. D. Stranks, R. H. Friend, M. G. Kanatzidis, A. D. Mohite, *Adv. Mater.* **2018**, *30*, 1704217.
[5] H. Zhang, Y. Wu, Q. Liao, Z. Zhang, Y. Liu, Q. Gao, P. Liu, M. Li, J. Yao, H. Fu, *Angew. Chem., Int. Ed.* **2018**, *57*, 7748.
[6] H. Chen, Y. Li, D. Xue, *Sci. China: Technol. Sci.* **2022**, *65*, 244.
[7] H. Fang, J. Yang, S. Adjokatse, E. Tekelenburg, M. E. Kamminga, H. Duim, J. Ye, G. R. Blake, J. Even, M. A. Loi, *Adv. Funct. Mater.* **2020**, *30*, 1907979.
[8] C. Song, H. Yang, F. Liu, G. J. Cheng, *Nat. Commun.* **2021**, *12*, 4879.
[9] J. Wang, C. Ge, E.-J. Guo, X. Xu, C. Wang, K. Jin, *Sci. China: Technol. Sci.* **2020**, *63*, 874.
[10] D. Ramirez, J. I. Uribe, L. Francaviglia, P. Romero-Gomez, A. Fontcuberta i Morral, F. Jaramillo, *J. Mater. Chem. C* **2018**, *6*, 6216.
[11] Z. Gan, Y. Cheng, W. Chen, K. P. Loh, B. Jia, X. Wen, *Adv. Sci.* **2021**, *8*, 2001843.
[12] S. Kahmann, H. Duim, H.-H. Fang, M. Dyksik, S. Adjokatse, M. R. Medina, M. Pitaro, P. Plochocka, M. A. Loi, *Adv. Funct. Mater.* **2021**, *31*, 2103778.
[13] W. Huang, Y. Liu, S. Yue, L. Zhu, P. Jin, Q. Wu, Y. Zhang, S. Qu, Z. Wang, Y. Chen, *Sci. China: Technol. Sci.* **2018**, *61*, 886.
[14] M. D. Smith, H. I. Karunadasa, *Acc. Chem. Res.* **2018**, *51*, 619.
[15] E. R. Dohner, E. T. Hoke, H. I. Karunadasa, *J. Am. Chem. Soc.* **2014**, *136*, 1718.
[16] S. Pathak, N. Sakai, F. Wisnivesky Rocca Rivarola, S. D. Stranks, J. Liu, G. E. Eperon, C. Ducati, K. Wojciechowski, J. T. Griffiths, A. A. Haghighirad, A. Pellaroque, R. H. Friend, H. J. Snaith, *Chem. Mater.* **2015**, *27*, 8066.
[17] J. Li, H. Wang, D. Li, *Front. Guided Wave Opt. Optoelectron.* **2020**, *13*, 225.
[18] G. Zhou, B. Su, J. Huang, Q. Zhang, Z. Xia, *Mater. Sci. Eng., R* **2020**, *141*, 100548.
[19] L. Zhang, L. Wu, K. Wang, B. Zou, *Adv. Sci.* **2019**, *6*, 1801628.
[20] R. Gautier, F. Massuyeau, G. Galnon, M. Paris, *Adv. Mater.* **2019**, *31*, 1807383.
[21] E. R. Dohner, A. Jaffe, L. R. Bradshaw, H. I. Karunadasa, *J. Am. Chem. Soc.* **2014**, *136*, 13154.
[22] R. Gautier, M. Paris, F. Massuyeau, *J. Am. Chem. Soc.* **2019**, *141*, 12619.
[23] D. Cortecchia, J. Yin, A. Petrozza, C. Soci, *J. Mater. Chem. C* **2019**, *7*, 4956.
[24] P. Klement, N. Dehnhardt, C.-D. Dong, F. Dobener, S. Bayliff, J. Winkler, D. M. Hofmann, P. J. Klar, S. Schumacher, S. Chatterjee, J. Heine, *Adv. Mater.* **2021**, *33*, 2100518.
[25] T. Li, X. Chen, X. Wang, H. Lu, Y. Yan, M. C. Beard, D. B. Mitzi, *ACS Energy Lett.* **2020**, *5*, 347.
[26] T. Hu, M. D. Smith, E. R. Dohner, M.-J. Sher, X. Wu, M. T. Trinh, A. Fisher, J. Corbett, X.-Y. Zhu, H. I. Karunadasa, A. M. Lindenberg, *J. Phys. Chem. Lett.* **2016**, *7*, 2258.
[27] R. T. Williams, K. S. Song, *J. Phys. Chem. Solids* **1990**, *51*, 679.
[28] S. Kahmann, E. K. Tekelenburg, H. Duim, M. E. Kamminga, M. A. Loi, *Nat. Commun.* **2020**, *11*, 2344.
[29] J. Yu, J. Kong, W. Hao, X. Guo, H. He, W. R. Leow, Z. Liu, P. Cai, G. Qian, S. Li, X. Chen, X. Chen, *Adv. Mater.* **2019**, *31*, 806385.
[30] W. Paritmongkol, E. R. Powers, N. S. Dahod, W. A. Tisdale, *J. Phys. Chem. Lett.* **2020**, *11*, 8565.
[31] A. Yangui, D. Garrot, J. S. Lauret, A. Lusson, G. Bouchez, E. Deleporte, S. Pillet, E. E. Bendeif, M. Castro, S. Triki, Y. Abid, K. Boukheddaden, *J. Phys. Chem. C* **2015**, *119*, 23638.
[32] B. Hu, J. Zhang, X. Zhu, M. Wang, B. Hu, *Nat. Commun.* **2020**, *11*, 2618.
[33] J. Liao, Z. Zhang, J. Wei, Z. Zhang, B. Wang, L. Zhou, G. Xing, Z. Tang, D. Kuang, *Adv. Opt. Mater.* **2022**, *10*, 2102426.
[34] F. Hao, C. C. Stoumpos, R. P. H. Chang, M. G. Kanatzidis, *J. Am. Chem. Soc.* **2014**, *136*, 8094.
[35] W. Qiu, Z. Xiao, K. Roh, N. K. Noel, A. Shapiro, P. Heremans, B. P. Rand, *Adv. Mater.* **2019**, *31*, 1806105.
[36] S. Gu, R. Lin, Q. Han, Y. Gao, H. Tan, J. Zhu, *Adv. Mater.* **2020**, *32*, 1907392.
[37] Y. Zhang, X. Liu, H. Sun, J. Zhang, X. Gao, C. Yang, Q. Li, H. Jiang, J. Wang, D. Xu, *Angew. Chem., Int. Ed.* **2021**, *60*, 7587.
[38] I. Zimmermann, S. Aghazada, M. K. Nazeeruddin, *Angew. Chem., Int. Ed.* **2019**, *58*, 1072.
[39] C. Qin, F. Zhang, L. Qin, X. Liu, H. Ji, L. Li, Y. Hu, Z. Lou, Y. Hou, F. Teng, *Adv. Electron. Mater.* **2021**, *7*, 2100384.
[40] M. Pitaro, E. K. Tekelenburg, S. Shao, M. A. Loi, *Adv. Mater.* **2022**, *34*, 2105844.
[41] M. Wei, K. Xiao, G. Walters, R. Lin, Y. Zhao, M. I. Saidaminov, P. Todorović, A. Johnston, Z. Huang, H. Chen, A. Li, J. Zhu, Z. Yang, Y. K. Wang, A. H. Proppe, S. O. Kelley, Y. Hou, O. Voznyy, H. Tan, E. H. Sargent, *Adv. Mater.* **2020**, *32*, 1907058.
[42] S. Kahmann, Z. Chen, O. Hordiichuk, O. Nazarenko, S. Shao, M. V. Kovalenko, G. R. Blake, S. Tao, M. A. Loi, *ACS Appl. Mater. Interfaces* **2022**, *14*, 34253.
[43] V. S. Chirvony, S. González-Carrero, I. Suárez, R. E. Galian, M. Sessolo, H. J. Bolink, J. P. Martínez-Pastor, J. Pérez-Prieto, *J. Phys. Chem. C* **2017**, *121*, 13381.
[44] H. Hu, Y. Liu, Z. Xie, Z. Xiao, G. Niu, J. Tang, *Adv. Opt. Mater.* **2021**, *9*, 2101423.
[45] B. Li, B. Chang, L. Pan, Z. Li, L. Fu, Z. He, L. Yin, **2020**, *5*, 3752.
[46] H.-H. Fang, S. Adjokatse, S. Shao, J. Even, M. A. Loi, *Nat. Commun.* **2018**, *9*, 243.
[47] S. Shao, J. Liu, G. Portale, H.-H. Fang, G. R. Blake, G. H. ten Brink, L. J. A. Koster, M. A. Loi, *Adv. Energy Mater.* **2017**, *7*, 1702019.
[48] T. Yokoyama, D. H. Cao, C. C. Stoumpos, T.-B. Song, Y. Sato, S. Aramaki, M. G. Kanatzidis, *J. Phys. Chem. Lett.* **2016**, *7*, 776.
[49] J. Dong, S. Shao, S. Kahmann, A. J. Rommens, D. Hermida-Merino, G. H. ten Brink, M. A. Loi, G. Portale, *Adv. Funct. Mater.* **2020**, *30*, 2001294.
[50] A. Karmakar, A. Bhattacharya, G. M. Bernard, A. Mar, V. K. Michaelis, *ACS Mater. Lett.* **2021**, *3*, 261.
[51] Z. Chen, G. Brocks, S. Tao, P. A. Bobbert, *Nat. Commun.* **2021**, *12*, 2687.
[52] Q. Gao, H. Sahin, J. Kang, S. Wei, *Phys. Rev. B* **2021**, *104*, 064204.
[53] G. Kresse, J. Hafner, *Phys. Rev. B* **1993**, *47*, 558.
[54] G. Kresse, J. Furthmüller, *Comput. Mater. Sci.* **1996**, *6*, 15.
[55] G. Kresse, J. Furthmüller, *Phys. Rev. B* **1996**, *54*, 11169.
[56] H. Peng, Z.-H. Yang, J. P. Perdew, J. Sun, *Phys. Rev. X* **2016**, *6*, 41005.
[57] P. E. Blöchl, *Phys. Rev. B* **1994**, *50*, 17953.
[58] K. Du, Q. Tu, X. Zhang, Q. Han, J. Liu, S. Zauscher, D. B. Mitzi, *Inorg. Chem.* **2017**, *56*, 9291.
[59] J. A. Van Vechten, T. K. Bergstresser, *Phys. Rev. B* **1970**, *1*, 3351.
[60] R. Hill1, D. Richardson, *J. Phys. C: Solid State Phys.* **1971**, *4*, L339.
[61] S.-H. Wei, A. Zunger, *Phys. Rev. B* **1991**, *43*, 1662.